Structure and sources of disorder in poly(3-hexylthiophene) crystals investigated by density functional calculations with van der Waals interactions

Weiyu Xie, Y. Y. Sun, S. B. Zhang, and John E. Northrup

Phys. Rev. B **83**, 184117 — Published 26 May 2011

DOI: 10.1103/PhysRevB.83.184117

Structure and sources of disorder in poly(3-hexylthiophene) crystals investigated by density-functional calculations with van der Waals interactions

Weiyu Xie,[1] *Y. Y. Sun*,[1] *S. B. Zhang*,[1] *John E. Northrup*[2]

[1]Department of Physics, Applied Physics, and Astronomy, Rensselaer Polytechnic Institute, Troy, NY 12180

[2]Palo Alto Research Center, 3333 Coyote Hill Road, Palo Alto, CA 94304

ABSTRACT

The crystal structure of poly(3-hexylthiophene) (P3HT) has been studied by first-principles calculations based on density functional theory. The generalized gradient approximation is employed and van der Waals interactions are treated accurately by the recently proposed local atomic potential approach. A variety of different models were tested, and the model having the lowest energy is a non-interdigitated structure having an orthorhombic cell with a = 17.2 Å, b = 7.7 Å, and c = 7.8 Å, where a, b, and c are the lengths of the lattice vectors perpendicular to the lamellae, in the π-π stacking direction, and along the thiophene backbone, respectively. These values are in reasonably good agreement with experiment. The P3HT polymer is not invariant under inversion and therefore exhibits directionality. Our calculations suggest that a likely structural defect occurring in P3HT is one in which one of the polymer backbones within a lamella runs in the direction opposite to the majority. Such defects may form in the process of self-assembly of the non-interdigitated lamellae and may be an important source of π-π stacking disorder. A possible explanation for a recently observed structural phase transition in polythiophene is proposed.

PACS: 61.66.Hq, 61.72.Bb, 64.60.Ej

1. INTRODUCTION

Poly(3-hexylthiophene) (P3HT) is a prototypical organic semiconductor that has been widely employed in photovoltaic and field-effect electronic devices.[1-8] P3HT is member of the poly(3-alkylthiophene) family, where each member is distinguished by the number of C atoms n in the alkyl side-chain (C_nH_{2n+1}). These alkyl side-chains are added to promote solubility, essential for the solution processing that enables large-scale low-cost applications. The polymerized thiophene rings constitute the polymer backbone, as shown in Fig. 1. Charge transport would be relatively fast along the polymer backbone because of the π-conjugation, which gives rise to large energy dispersion of the holes and electrons along the chains. However, charge transport along this pathway is limited by the finite length of the polymer. Neighboring polymer chains interact strongly via π-π interaction between the thiophene rings and by van der Waals (vdW) interaction between the alkyl side-chains. These interactions give rise to two-dimensional sheets (lamellae) with ordering of the polymer backbones along the π-stacking direction. Transport within a lamella is enabled by the delocalization of the carriers in the π-stacking direction.[9] Interactions between the alkyl side-chains emanating from neighboring lamellae can give rise to ordered stacking in the third dimension, thereby forming P3HT crystals. The third dimension has no direct contribution to carrier transport. Although P3HT polymer chains with predominantly head-to-tail ordering (regioregular P3HT) can now be routinely synthesized,[10] a complete and detailed picture of the molecular stacking and internal structure of three-dimensional crystals remains elusive after two-decades of study.[11-16] Experimental determination of the P3HT crystal structure is made difficult by the large number of structural parameters and the low crystallinity that is common for polymeric materials.

In this paper we report first-principles calculations based on density functional theory (DFT) that are intended to determine the minimum energy P3HT structure at $T = 0$. The generalized

gradient approximation is employed and van der Waals (vdW) interactions are treated accurately by the recently proposed local atomic potential (LAP) approach. A variety of different models were tested, and the model having the lowest energy is a non-interdigitated structure having an orthorhombic cell with a = 17.2 Å, b = 7.7 Å, and c = 7.8 Å, where a, b, and c are the lengths of the lattice vectors perpendicular to the lamellae, in the π-π stacking direction, and along the thiophene backbone, respectively. These values are in reasonably good agreement with experiments.

The P3HT polymer is not invariant under inversion and therefore exhibits directionality. Our calculations suggest that a likely structural defect occurring in P3HT is one in which one of the polymer backbones within a lamella runs in the direction opposite to the majority, as illustrated in Fig. 1(c). Such defects may form in the process of self-assembly of the non-interdigitated lamellae and may be an important source of π-π stacking disorder.

2. COMPUTATIONAL METHOD

Some previous theoretical modeling of the P3HT crystal structure has employed empirical force field calculations.[15] Recently, density-functional theory (DFT) has been used to study the structure.[17-20] In the P3HT crystal the alkyl side-chain interactions arise primarily from van der Waals interactions, and so it is desirable to employ a theoretical approach that treats these interactions more accurately than is possible in standard DFT. We therefore employ a recently developed method known as the DFT plus local atomic potential (DFT+LAP) method. This method includes the vdW interaction accurately without requiring significant extra computational cost beyond standard DFT calculations.

In the DFT+LAP method,[21] the vdW interaction is approximately described by the LAPs that are centered at individual atom sites. The LAPs are added to the local part of the pseudopotential for each element so that the method is completely compatible with standard DFT

calculations. Here, we upgrade our previous implementation of LAPs so that Vanderbilt-type ultrasoft pseudopotentials[22] may be employed rather than norm-conserving pseudopotentials. The LAP parameters for C and H are obtained from Ref. 21. For S, we obtain the LAP parameters ($c_0 = 1.35\times10^3$ Ry·Bohr^8, $n = 8$, $v_{const} = 0.55 \times 10^{-3}$ Ry) using the S_2 dimer following the procedure described in Ref. 21. The revised Perdew-Burke-Ernzerhof approximation[23] to the exchange-correlation functional is adopted. Plane waves with kinetic energies less than a cutoff energy of 544 eV (40 Ry) are included in the basis set. A unit cell containing two backbone chains (100 atoms per cell, 25 atoms per monomer) is used in our calculations. The Brillouin zone is sampled by a Monkhorst-Pack type[24] 1×4×4 *k*-point grid. The combination of the cutoff energy and *k*-point sampling employed here is checked to give accuracy of about 3 meV/monomer in total-energy difference. All atoms are relaxed until the forces are smaller than 25 meV/Å. For variable cell relaxations, the residual stress on the cell is required to be smaller than 0.5 kBar. The Quantum-ESPRESSO program[25] is employed to perform the DFT+LAP calculations.

To check the accuracy of the DFT+LAP method we performed highly accurate quantum chemistry calculations using the MOLPRO program[26] for the two benchmark systems shown in Fig. 2. The thiophene dimer and ethane dimer represent the interactions between thiophene backbones and between alkyl side-chains, respectively. The thiophene dimer is in a parallel configuration and the inter-plane distance is fixed at 3.4 Å [see Fig. 2(a)]. The accurate benchmark results are obtained by CCSD(T) corrected complete basis set MP2 calculations,[27, 28] where MP2 and CCSD(T) stand for Møller-Plesset second-order perturbation theory and coupled-cluster theory with single, double, and perturbative triple excitations, respectively. The complete basis set MP2 results are obtained by extrapolation using the aug-cc-pVTZ and aug-cc-pVQZ Gaussian-type basis set. The CCSD(T) corrections, which account for higher-order

correlation energies, are obtained using the aug-cc-pVTZ basis set. The good agreement between the DFT+LAP and accurate benchmark results, as depicted in Fig. 2, indicates that the DFT+LAP method can provide an accurate description for both the vdW and π-π stacking systems. Both the equilibrium distances and the binding energies can be accurately obtained from the DFT+LAP calculations.

3. STRUCTURAL MODELS OF P3HT CRYSTAL

The structure of P3HT crystal is characterized by the unit cell parameters and a set of internal parameters.[11, 12, 16-20, 29] Here, following the convention, we use ***a***, ***b***, and ***c*** to denote the lattice vectors along the lamella stacking, π-π stacking, and thiophene backbone, respectively. The lengths of ***a***, ***b***, and ***c*** are denoted by *a*, *b*, and *c*, respectively. The unit cell of P3HT has been proposed to be either orthorhombic[15] with the angle γ (between lattice vectors ***a*** and ***b***) of 90° or monoclinic[16, 29, 30] with a γ slightly away from the right angle by 3 to 4°. Each cell contains two polymer chains displaced from each other by ~0.5*b* along the π-π stacking direction, ***b***. We consider structures in which these two polymers are shifted relative to each other along the ***c*** direction by various distances δ_c.

As illustrated in Fig. 3, the internal structure of P3HT may be specified in terms of various parameters: 1) θ_1 is the tilt angle, in the projection along the ***c***-vector, of the thiophene plane away from the lamella plane normal (i.e., the direction of ***a***-vector in the case of orthorhombic cell). 2) θ_2 is the angle, in the projection along the ***c***-vector, between the alkyl side-chain and the lamella plane normal. 3) θ_3 is the angle, in the projection along the ***b***-vector, between the alkyl side-chain and the lamella plane normal. 4) θ_4 is the alkyl side-chain torsion angle around the C-C σ-bond connecting the thiophene ring and the side-chain. 5) δ_c is the registry shift of two adjacent backbones along the ***c***-vector. (δ_c=0 is the eclipsed configuration of thiophene rings.)

We also consider another degree of freedom: the *directionality* of the thiophene backbone. In regioregular head-to-tail P3HT polymer chain the alkyl-chains may be attached all on the left side or all on the right side of the thiophene rings. We refer to the former as an L chain and the latter as an R chain (see Fig. 1). A lamella may be formed as an ordered array of L chains or an ordered array of R chains. These two lamellae would be structurally equivalent. However it is also possible to form a lamella with an ordered mixture of L and R chains. One possibility is the structure with a two-chain cell having one L chain and one R chain. Two basic stacking sequences possible within a two-chain cell are LL and LR as illustrated in Figs. 3(c) and 3(d). There is no simple route to convert an LR structure into an LL structure. It is not clear whether the process of self assembly will always lead to the stacking sequence which minimizes the energy. Thus the directionality of polymer chains in P3HT may be an important source of structural disorder.

Now we consider the structural models of P3HT that may be obtained by variation of the parameters discussed above. The tilt angle θ_1 is mainly driven by the electrostatic interactions between the thiophene rings on adjacent backbones.[31] The value of the tilt angle θ_1 may be determined by energy minimization. Since θ_2 and θ_3 arise from the rotations about the C-C σ-bonds in the side-chain, mainly about the bond connecting the thiophene ring and the side-chain (i.e., θ_4), we only consider θ_4 in this work. For an isolated backbone it has been shown that there exist two stable configurations with $\theta_4 \approx 0°$ and $\theta_4 \approx 90°$.[20] In a P3HT crystal the transition from a structure with $\theta_4 \approx 0°$ to one with $\theta_4 \approx 90°$ requires surmounting a high energy barrier. This transition will not occur spontaneously in the computational energy minimization process. Therefore we treat structures with $\theta_4 \approx 0°$ and $\theta_4 \approx 90°$ as two distinct models, and classify them as Model I ($\theta_4 \approx 0°$) and Model II ($\theta_4 \approx 90°$), respectively. For each model, we consider the two basic stacking sequences, i.e., LL and LR. We consider structures with δ_c varying from 0 to c for

all the cases. The four basic types of models, I(LL), I(LR), II(LL), and II(LR) are illustrated in Figs. 4(a)-(d), respectively. In addition to these four models, we consider another model proposed recently by Kayunkid *et al* on the basis of electron diffraction experiments.[29] This model is similar to I(LR), but has a wavy shape structure if viewed along the ***c***-vector. Also, a value of $\delta_c \approx 0.8c$ has been proposed for this model. We will refer to this structure as Model III. It is depicted in Figs. 5(a) and 5(b).

4. RESULTS AND DISCUSSION

Figure 6 shows the results from DFT+LAP calculations on all the models discussed in the previous section. The calculated structural parameters are listed in Table 1. Figure 6(a) shows the total energies as a function of δ_c. For Model I and II, only the results for the structures with lower total energy between the LL and LR variations are shown. The results for the LL variation are marked as solid symbols, while the results for the LR variation are marked as open symbols. For Model III, following the original proposal, we consider only the case having $\delta_c \approx 0.8c$ and the LR stacking sequence.[29] From Fig. 6(a), it can be seen that Model I is stabilized at $\delta_c \approx 0$, while Model II is stabilized at δ_c ranging from $0.3c$ to $0.5c$. Among all the models that we have considered, model I ($\theta_4 \approx 0°$) having $\theta_1 \approx 26°$ and $\delta_c \approx 0$, with the LL stacking sequence has the lowest energy.

It is worth noting that the structure of Model III changes considerably after variable-cell relaxation and the wavy shape structure that was present in the starting configuration disappears, as shown in Fig. 5(c). After relaxation this structure is about 101 meV/monomer higher than the most stable structure. Model II, with $\delta_c \approx 0.5c$, has a total energy that is about 58 meV/monomer higher than the best Model I.

For both Model I and II, the energy of the LR variation is only slightly higher than the LL variation. This indicates that stacking faults, for example the structure with a stacking sequence

...LLL**R**LLL…, as illustrated in Fig. 1(c), could have a low formation energy and may form readily in the process of self-assembly of solution processed P3HT crystals. Based on calculations with four chains per cell we estimate the formation energy of such a fault to be ~30 meV/monomer in the bulk. However, the incorporation of such a stacking fault should probably be considered as a process taking place at the (010) surface of a growing lamella, and in that case the defective structure (…LLLR) would likely be higher in energy than the ideal structure (…LLLL) by a lesser amount, perhaps on the order of ~15 meV/monomer. A detailed study of the kinetics of formation is outside the scope of the present investigation.

Figure 6(b) shows the length of the ***a***-vector (a) of the three models as a function of δ_c. The experimentally measured a is between 16.0 and 16.8 Å, which indicates that there is little interdigitation between alkyl side-chains from adjacent lamellae. The calculated values of a for Model I at $\delta_c \approx 0$ and Model II at $\delta_c \approx 0.5c$ are 17.2 and 17.1 Å, respectively. These values are in good agreement with experiment. Also, for both models, no interdigitation occurs at their respective equilibrium values of δ_c (i.e., 0 for Model I and $0.5c$ for Model II). Model III, however, has a significantly larger a in comparison to the other two models. The reason can be seen from Fig. 5(c), which shows that after full variable-cell relaxation, Model III is stabilized at $\theta_1 \approx 0$. Without the tilting by θ_1 and without side-chain interdigitation, Model III must assume a larger a to optimize the interaction between alkyl side-chains in neighboring lamellae.

Figure 6(c) shows the length of the ***b***-vector (b) as a function of δ_c. The experimentally determined value of b is between 7.66 and 7.8 Å.[11, 29] Our calculation shows that Model I has b = 7.70 Å at $\delta_c \approx 0$, which is within the range of measured values. In contrast to Model I, both Model II and Model III have equilibrium values of b that lie outside the range of experimentally measured values.

A recent experiment has reported a possible phase change involving an abrupt shrinkage of b (by about 3%) after annealing the sample at high temperature.[32] It is interesting to note that for our lowest energy structure, I(LL) (δ_c = 0), we find a reduction in b by about 4.6% when δ_c is increased from 0 to 0.5c. Specifically, for I(LL) (δ_c = 0) we obtained b = 7.7 Å, and for I(LL) (δ_c = 0.5c) we find b = 7.3 Å. Model II(LL) (δ_c = 0.5c) also exhibits a reduced value of b (~7.1 Å). It is tempting therefore to propose that the experimentally observed reduction in b at higher temperature (T > 100°) may also involve a simultaneous change in δ_c. This explanation for the change in structure appears plausible because structures having δ_c = 0.5c allow greater freedom for motion of the alkyl side-chains and so may be stabilized by the entropic contribution to the free energy at higher temperatures.

Figure 6(d) shows the change of the angle γ as a function of δ_c for the three models. Experimentally, the value of γ is found to be either 90°, corresponding to an orthorhombic lattice,[15] or an angle slightly off the right angle, e.g., 86.5°, indicative of a monoclinic lattice.[29] Our calculation shows that Model I at δ_c = 0 is stabilized at γ= 90°, while Model II at $\delta_c \approx 0.5c$ is stabilized at γ = 101°. Note that the most stable configurations found in Refs. 19 and 20 are similar to Model II(LL) (δ_c = 0.5c), but with γ= 90°, which has a total-energy 19 meV/monomer higher than that with γ= 101° according to our calculation.

Overall, our DFT+LAP results show that Model I(LL) (δ_c = 0) is energetically the most favorable, followed by Model II (higher by 58 meV/monomer) and Model III (higher by 101 meV/monomer). Model I(LL) (δ_c = 0) also shows good agreement with experiment for the lattice parameters a, b, and γ.

To gain insight into the relation between the structure and relative stability of Models I and II, we estimated the thiophene-thiophene interaction (π-π stacking) by removing the side-chains,

and the side-chain—side-chain interaction (vdW) by removing the backbones. In both calculations, the broken bonds are passivated by H atoms. These calculations are performed using the "as-is" structure without further atomic relaxation. The results show that the greater stability of Model I compared to II arises both from more favorable interactions between the alkyl side-chains and from a more favorable thiophene-thiophene interaction. Roughly, two thirds of the 58 meV/monomer difference in the total-energy comes from the stronger alkyl side-chain interactions in Model I.

We note that for an isolated thiophene dimer, our LAP calculations show that the configuration with the two rings oppositely oriented, as in Model II, is slightly more stable than the displaced parallel configuration by 2 meV per thiophene, consistent with previous CCSD(T)-corrected MP2 results.[33] Interestingly, in P3HT crystals, with the constraints of the alkyl side-chains the parallel configuration as in Model I, becomes more stable. Moreover, our LAP calculations on polyethylene (i.e., infinite long side-chain) show that the structure with two chains per unit cell,[34] similar to Model II, is more stable than that with a single chain per unit cell, as in Model I, by 27 meV per chain unit. However, with the constraints on the spacing and registry shift between alkyl side-chains, which are set by the presence of thiophene backbones, the polyethylene structure with a single chain per cell becomes more stable by about 12 meV per chain unit. These results manifest the importance of the structural constraints on the final adopted structure. Since different derivatives of polythiophene may have different side-chain spacing, side-chain length and the abovementioned LR symmetry in the backbone, each individual material may adopt a different structure in a variety of aspects, such as interdigitation, side-chain rotation, registry shift in the backbone.

5. CONCLUSIONS

In summary, we have investigated the crystal structure of P3HT using the DFT+LAP method, which gives accurate descriptions for both the π-π stacking between thiophene rings and the van der Waals component of the interaction between alkyl side-chains. Our calculations show that interactions between the alkyl side-chains on neighboring polymer chains play an important role in determining the equilibrium structure. Of the structures that we have considered the one having the lowest energy may be characterized by an orthorhombic lattice (γ = 90°), with torsion angle $\theta_4 \approx 0°$, backbone tilt angle $\theta_1 \approx 26°$, registry shift $\delta_c \approx 0$, and with the LL stacking sequence. We term this model I(LL) ($\delta_c \approx 0$). No significant interdigitation of alkyl side-chains occurs in this structure. Good agreement with experimental measurements of the lattice parameters *a*, *b*, and γ is obtained for this model. Two types of ordered sequences (LL vs. LR) of thiophene backbones were studied. For $\delta_c = 0$, the cell with LR type stacking is higher in energy than the LL type stacking by 60 meV/cell. In the regions of δ_c from 0.2*c* to 0.6*c*, however, LR type stacking could become energetically favorable. Based on these results we suggest that stacking faults may exist in the solution processed P3HT crystals, and may represent an important source of structural disorder. In addition we proposed a possible explanation for the bimodal distribution in the P3HT π-π stacking distance that was reported recently.[32]

ACKNOWLEDGMENT

This work was supported by the US Department of Energy under Grant No. DE-SC0002623. Supercomputer time was provided by the CCNI at RPI. Work at the Palo Alto Research Center (PARC) was supported by the AFOSR under Grant No. FA9550-09-1-0436.

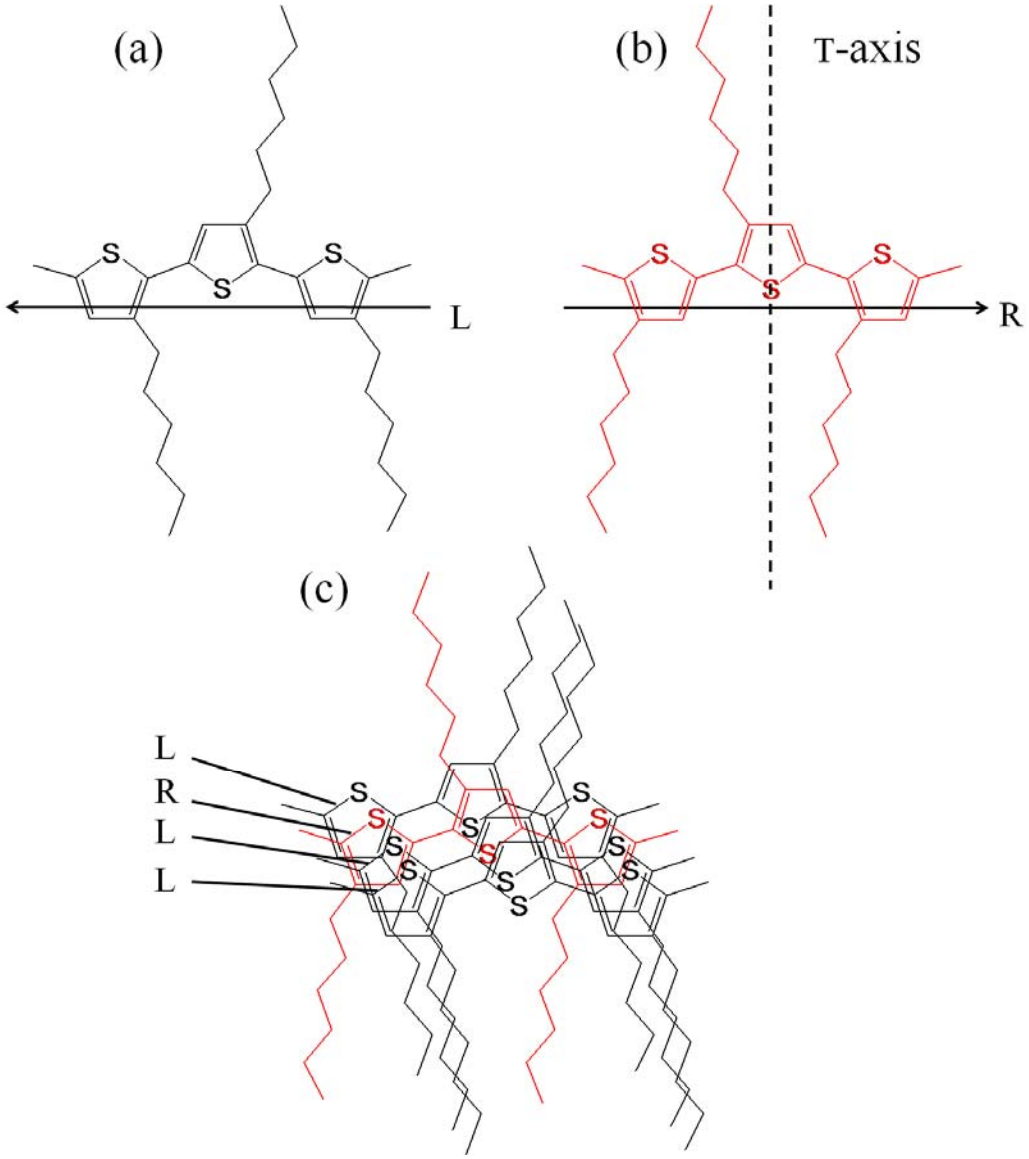

FIG. 1. (color online) Regioregular head-to-tail alkyl-substituted polythiophene. (a) and (b) are schematic representations of structures defining the L (a) and R (b) backbone chains. L can be converted into R by a 180° rotation around the T axis. (c) This depicts a stacking fault, where an R chain has been inserted into a lamella consisting of L chains. Such defects could form in the process of self-assembly out of solution and could be an important source of structural disorder.

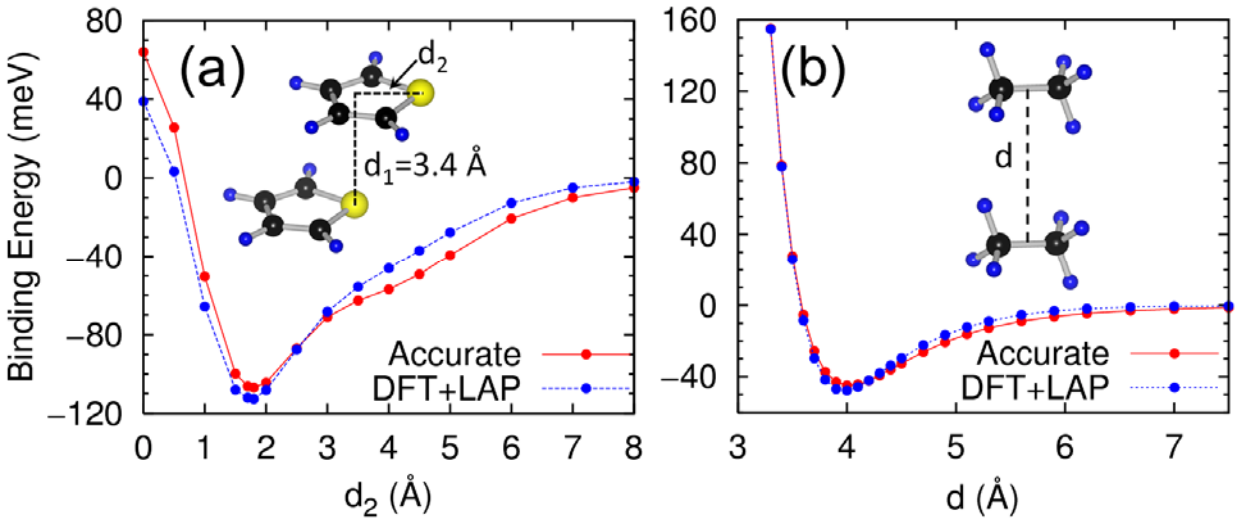

FIG. 2. (color online) CCSD(T) and DFT+LAP calculations for benchmark systems (a) parallel thiophene dimer, and (b) parallel ethane dimer. The insets show the structures of the dimers, where C, H, and S are represented by black, blue and yellow balls, respectively.

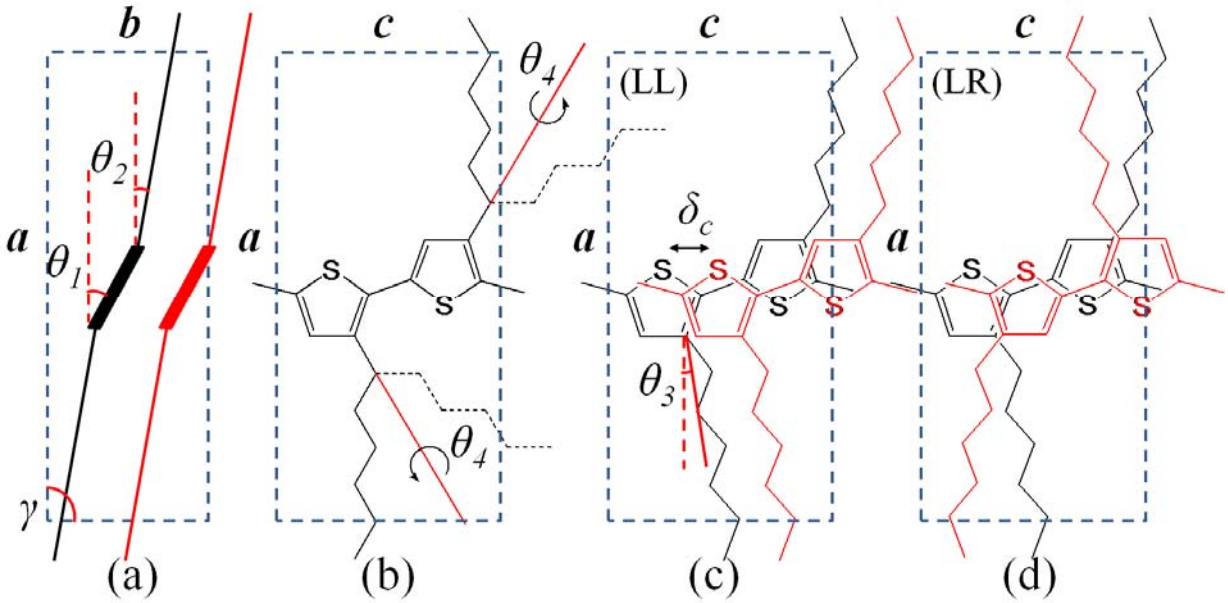

FIG. 3. (color online) Define (a) a, b, θ_1, θ_2, and γ, (b) c and θ_4; (c) θ_3, δ_c and stacking sequence LL; (d) stacking sequence LR.

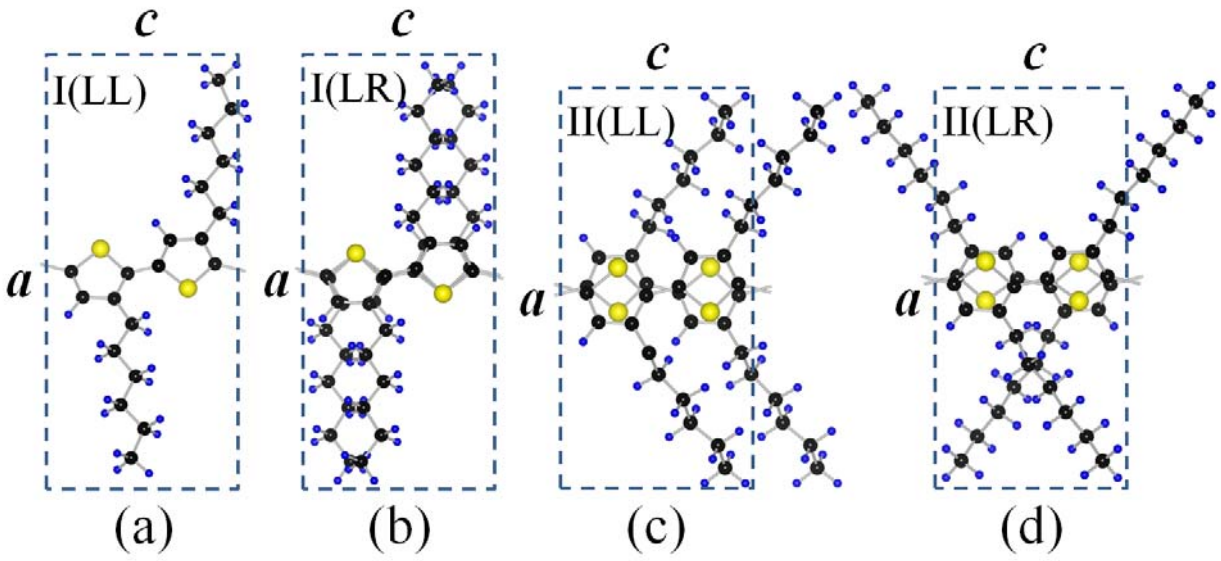

FIG. 4. (color online) (a) Model I(LL) at δ_c=0, (b) Model I(LR) at δ_c=0, (c) Model II(LL) at δ_c=0.5c, (d) Model II(LR) at δ_c=0.5c.

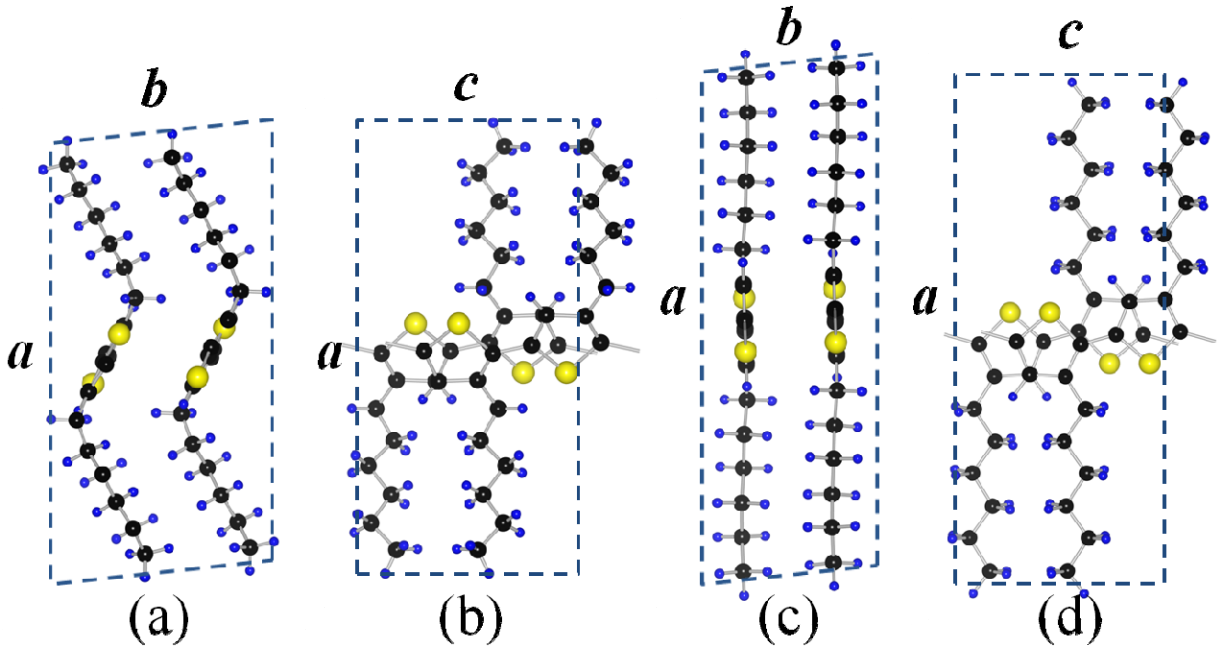

FIG. 5. (color online) Depiction of Model III prior to relaxation: (a) projection along ***c***-vector, (b) projection along ***b***-vector. Depiction of Model III after relaxation: (c) projection along ***c***-vector, (d) projection along ***b***-vector.

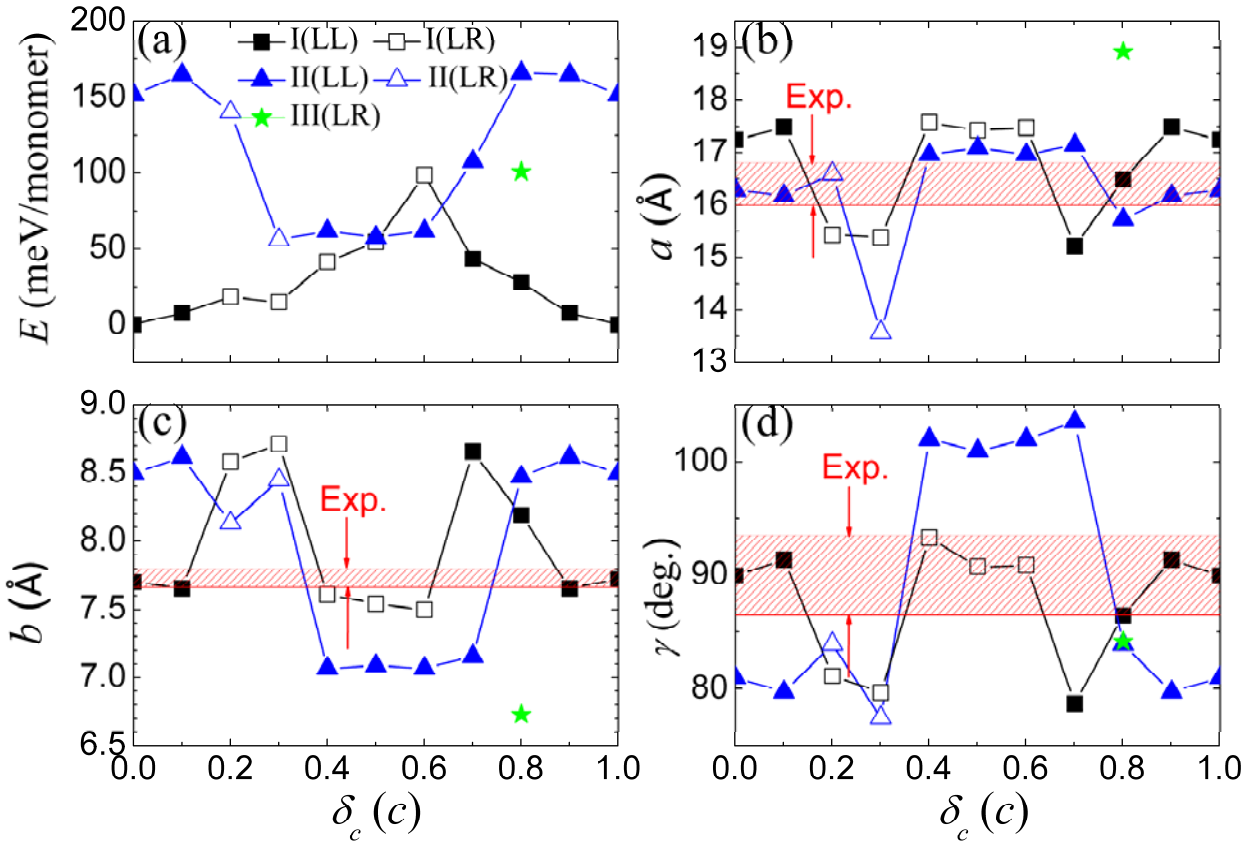

FIG. 6. (color online) Model I~III's (a) energy as function of δ_c, and corresponding (b) a, (c) b and (d) angle γ.

TABLE I. Structural parameters of P3HT crystals obtained in this work and previous studies.

	a [nm]	b [nm]	c [nm]	γ [deg.]	θ_1 [deg.]	θ_2 [deg.]	θ_3 [deg.]	θ_4 [deg.]	δ_c [c]
I(LL)	1.724	0.770	0.780	90	26.5	20.5	0.6	1.7	0
II(LL)	1.709	0.709	0.780	101	19.2	-21.5	35.8	93.3	0.5
III(LR)	1.891	0.673	0.780	84	3.8	8.0	0.3	5.1	0.8
Calculation[18]	--	0.76	0.76	90	23	--	0	0	0
Calculation[20]	1.676	0.781	0.770	90	29.2	--	--	97.6	0.5
Calculation[19]	1.582	0.684	0.783	90	6.9	39.2	34.1	--	0.5
Experiment[15]	1.663	0.775	0.77	90	--	--	--	--	--
Experiment[11]	1.68	0.766	0.77	--	5	--	--	89	0.5
Experiment[29]	1.60	0.78	0.78	86.5	29.5	32.5	0	--	0.8

REFERENCES

[1]Z. Bao, A. Dodobalapor and A. J. Lovinger, Appl. Phys. Lett. **69**, 4108 (1996).

[2]H. Sirringhaus, N. Tessler, R. H. Friend, Science **280**, 1741 (1998).

[3]H. Sirringhaus, P. J. Brown, R. H. Friend, M. M. Nielsen, K. Bechgaard, B. M. W. Langeveld-Voss, A. J. H. Spiering, R. A. J. Janssen, E. W. Meijer, P. Herwig, D. M. de Leeuw, Nature **401**, 685 (1999).

[4]R. J. Kline, M. D. McGehee, E. N. Kadnikova, J. S. Liu, J. M. J. Frechet, Adv. Mater. **15**, 1519 (2003).

[5]F. C. Krebs, S. V. Hoffmann, M. Jorgensen, Synth. Met. **138**, 471 (2003).

[6]H. C. Yang, T. J. Shin, L. Yang, K. Cho, C. Y. Ryu, Z. N. Bao, Adv. Funct. Mater. **15**, 671 (2005).

[7]D. H. Kim, Y. D. Park, Y. S. Jang, H. C. Yang, Y. H. Kim, J. I. Han, D. G. Moon, S. J. Park, T. Y. Chang, C. W. Chang, M. K. Joo, C. Y. Ryu, K. W. Cho, Adv. Funct. Mater. **15**, 77 (2005).

[8]R. Zhang, B. Li, M. C. Iovu, M. Jeffries-El, G. Sauve, J. Cooper, S. J. Jia, S. Tristram-Nagle, D. M. Smilgies, D. N. Lambeth, R. D. McCullough, T. Kowalewski, J. Am. Chem. Soc. **128**, 3480 (2006).

[9]R. A. Street, J. E. Northrup, A. Salleo, Phys. Rev. B **71**, 165202 (2005).

[10]Y. Kim, S. Cook, S. M. Tuladhar, S. A. Choulis, J. Nelson, J. R. Durrant, D. D. C. Bradley, M. Giles, I. McCulloch, C. S. Ha, M. Ree, Nature Mater. **5**, 197 (2006).

[11]T. J. Prosa, M. J. Winokur, J. Moulton, P. Smith, A. J. Heeger, Macromolecules **25**, 4364 (1992).

[12]K. Tashiro, Y. Minagawa, M. Kobayashi, S. Morita, T. Kawai, K. Yoshino, Jpn. J. Appl. Phys. **33**, L1023 (1994).

[13]K. Tashiro, M. Kobayashi, K. Morita, T. Kawai, K. Yoshino, Synth. Met. **69**, 397 (1995).

[14]T. J. Prosa, M. J. Winokur, J. Moulton, P. Smith, A. J. Heeger, Phys. Rev. B **51**, 159 (1995).

[15]K. Tashiro, M. Kobayashi, T. Kawai, K. Yoshino, Polymer **38**, 2867 (1997).

[16]M. Brinkmann, P. Rannou, Adv. Funct. Mater. **17**, 101 (2007).

[17]D. M. DeLongchamp, R. J. Kline, E. K. Lin, D. A. Fischer, L. J. Richter, L. A. Lucas, M. Heeney, I. McCulloch, J. E. Northrup, Adv. Mater. **19**, 833 (2007).

[18]J. E. Northrup, Phys. Rev. B **76**, 245202 (2007).

[19]A. Maillard, A. Rochefort, Phys. Rev. B **79**, 115207 (2009).

[20]S. Dag, L.-W. Wang, J. Phys. Chem. B **114**, 5997 (2010).

[21]Y. Y. Sun, Y. H. Kim, K. Lee, S. B. Zhang, J. Chem. Phys. **129**, 154102 (2008).

[22]D. Vanderbilt, Phys. Rev. B **41**, 7892 (1990).

[23]Y. Zhang, W. Yang, Phys. Rev. Lett. **80**, 890 (1998).

[24]T. Yamamoto, D. Komarudin, M. Arai, B. L. Lee, H. Suganuma, N. Asakawa, Y. Inoue, K. Kubota, S. Sasaki, T. Fukuda, H. Matsuda, J. Am. Chem. Soc. **120**, 2047 (1998).

[25]QUANTUM-ESPRESSO, Version 4.2, see http://www.quantum-espresso.org/.

[26]MOLPRO, Version 2006.1, see http://www.molpro.net.

[27]P. Jurecka, J. Sponer, J. Cerny, P. Hobza, Phys. Chem. Chem. Phys. **8**, 1985 (2006).

[28]Y. Y. Sun, K. Lee, L. Wang, Y.-H. Kim, W. Chen, Z. Chen, S. B. Zhang, Phys. Rev. B **82**, 073401 (2010).

[29]N. Kayunkid, S. Uttiya, M. Brinkmann, Macromolecules **43**, 4961 (2010).

[30]M. Brinkmann, P. Rannou, Macromolecules **42**, 1125 (2009).

[31]J. E. Northrup, M. L. Chabinyc, R. Hamilton, I. McCulloch, M. Heeney, J. Appl. Phys. **104**, 083705 (2008).

[32]S. Joshi, P. Pingel, S. Grigorian, T. Panzner, U. Pietsch, D. Neher, M. Forster, U. Scherf, Macromolecules **42**, 4651 (2009).

[33]S. Tsuzuki, K. Honda, R. Azumi, J. Am. Chem. Soc. **124**, 12200 (2002).

[34]K. Tashiro, I. Tanaka, T. Oohara, N. Niimura, S. Fujiwara, T. Kamae, Macromolecules **37**, 4109 (2004).